

Foam Au driven by $4\omega - 2\omega$ ignition laser pulse for inertial confinement fusion

Ke Lan and Peng Song

Institute of Applied Physics and Computational Mathematics, Beijing, 100094, China

Green light (2ω) has the potential to drive ignition target for laser fusion with significantly more energy than blue light (3ω) and a relatively higher damage threshold for the optic components in the final optic assembly, but it has issues of a relatively low laser to x-ray conversion efficiency and a hard x-ray spectrum as compared to 3ω . In this paper, we propose to drive a foam hohlraum wall with an ignition laser pulse by taking a 4ω laser at the pre-pulse and a 2ω laser at the main-pulse, called as $4\omega - 2\omega$ ignition pulse. This novel design has the following advantages: (1) benefiting from 2ω of its relatively high energy output and low damage threshold during main-pulse; (2) benefiting from foam in its relatively high laser to x-ray conversion efficiency and relatively low M-band fraction in re-emission; (3) benefiting from 4ω of its low LPI during pre-pulse. From our 1D simulations with Au material, the laser to x-ray conversion in a foam driven by $4\omega - 2\omega$ pulse has an increase of 28% as compared to a solid target driven by 3ω with the same pulse shape. The relatively thin optical depth of foam is one of the main reasons for the increase of laser to x-ray conversion efficiency inside a foam target.

PACS numbers: 52.70.La, 52.35.Tc, 47.40.Nm

I. INTRODUCTION

The choice of laser wavelength is central to the inertial confinement fusion (ICF) indirect-drive ignition study, because laser plasma instabilities (LPI) impacts a wide range of physics issues, such as hohlraum energetics, implosion symmetry and pulse shaping[1]. Present laser facilities designed for ICF study almost all operate at blue light (3ω), such as the National Ignition Facility[2], the Shenguang series [3, 4], the OAMEG[5] and the Laser Mégajoule facility [6], because 3ω has the advantages of a higher laser deposition[7, 8] and a lower LPI [9] than green light (2ω). However, 3ω is generated via the frequency-tripling technique with a relatively low efficiency, and in addition, it has a relatively low damage threshold for the optic components in the final optic assembly [10]. The two issues greatly limit the maximum energy output capability of a 3ω laser facility. In contrast, 2ω laser can highly increase the threshold for optical damages, which therefore results in a lower operation costs for a laser facility and a higher laser energy deliverable on target [11, 12]. Furthermore, in the long term, any reactor based on laser-driven ICF will require laser operation at sufficiently high wavelength for keeping the live time of the optics at a level that meets the energy production requirements [13]. In fact, a series experimental works with 2ω laser beams [14–17] have been performed, and they demonstrated that LPI aroused by 2ω is in an acceptable level for fusion experiments. Thus, 2ω may hold significant advantages for future ignition and high-fusion yield study and can be a laser wavelength competitive with 3ω for future ignition laser facility. Nevertheless, 2ω laser has a lower laser to X-ray conversion efficiency than 3ω due to its lower laser deposition and higher LPI backscatters, which therefore requires higher laser energy and power. These issues seriously block the use of 2ω for an ignition laser facility.

In indirect-drive ICF study, the energy coupling from laser to capsule can be described by three efficiency: the absorbed laser efficiency η_{aL} , the laser to x-ray conversion efficiency η_{LX} , and the hohlraum to capsule η_{HC} . Here, η_{aL} is decided

by the laser deposition via inverse bremsstrahlung process and the backscatters due to LPI, η_{LX} is decided by atomic processes, bremsstrahlung emission and its inverse process, and η_{HC} is decided by hohlraum geometrical parameters and albedos of hohlraum wall and capsule. Notice that η_{aL} and η_{LX} are related to both laser and target parameters, while η_{HC} is only connected to the target parameters including wall materials and geometrical configurations at a given radiation environment inside a hohlraum. At a longer laser wavelength λ_L , both η_{aL} and η_{LX} are lower, which is due to lower laser deposition and higher LPI for η_{aL} while due to thinner laser deposition depth for η_{LX} . As a result, for a given target, 2ω laser has a lower η_{aL} and a lower η_{LX} than 3ω and 4ω . However, both η_{aL} and η_{LX} are also connected to the target parameters, such the initial density ρ_0 , one can therefore consider to change ρ_0 to increase η_{aL} and η_{LX} at 2ω to make them be comparable with those at 3ω with a solid target.

In fact, it was predicted by HR analytical theory that the lower density hohlraum walls produce higher radiation temperature than the high density walls [18] because it can reduce hydrodynamic losses. According to HR theory, the radiation front propagates subsonically in materials with high density and part of the absorbed energy is wasted by the flow kinetic energy, while it propagates supersonic in the materials with lower density and can devote almost all of the absorbed energy to heating the material. From this theory, a foam target has a higher albedo, and it therefore has a higher η_{HC} than a solid target. This prediction was demonstrated successfully by later experiments with Ta₂O₅ foams[19] and Au foams[20–22] and numerical simulations with Au foams[23, 24]. Notice that above experimental and numerical comparisons of foam and solid were performed under the same lasers at 3ω . However, to explore the possibilities of 2ω laser for future ignition laser facilities, we need to know: how about the x-ray output of a foam Au target under a 2ω laser as compared to a solid Au target under 3ω ? It would be encouraging for 2ω laser if its x-ray output can be higher, or at least not lower, than 3ω . Otherwise, it would be discouraging for 2ω laser in ICF ap-

plication. In addition, the foams used in above comparisons have thicknesses covering both laser ablation region and radiation ablation region, which combines the influences of foam on η_{aL} , η_{LX} , and η_{HC} . We need to make clear if a foam can help to increase η_{aL} and η_{LX} at 2ω as compared to those of a solid target at 3ω or not.

In this paper, based on our one-dimensional simulations of x-ray output from Au targets with different ρ_0 driven by an ignition laser pulse with various λ_L , we propose to drive a foam hohlraum wall with an ignition laser pulse at 4ω during its pre-pulse and 2ω during main-pulse for in-direct drive ICF, called as 4ω - 2ω pulse hereafter. Here, it is worth to mention that 4ω laser has the highest η_{aL} and η_{LX} with the lowest LPI than 2ω and 3ω for the same target, but meanwhile, it has the lowest damage threshold for the optic components. To utmost utilize the advantages of 4ω laser to greatly inhibit the hydrodynamic instabilities aroused by LPI during pre-pulse, we therefore consider to use 4ω laser for the pre-pulse. Moreover, to make clear whether a foam can help to increase η_{aL} and η_{LX} at 2ω as compared to the case of a solid target at 3ω or not, we will use a foam-solid target, in which the foam part faces to laser source and has a thickness approximately equal to the laser ablated depth under the drive laser. The foam-solid target has the same areal density as the solid target.

The remaining presentation is organized as follows. In Sec. II, we will present the code and models used in this study. In Sec. III, we will discuss the simulation results of different models by comparing their laser to X-ray conversion efficiency and the M-band fraction, and we analyze the reasons why foam can help to increase the laser to x-ray conversion efficiency. Finally, we will present a summary in Sec. IV.

II. CODE AND MODEL

We use our one-dimensional (1D) multi-group radiation hydrodynamic code RDMG [25] to simulate the Au plane targets, foam or solid, under an ignition laser pulse. RDMG is widely used in both indirect-drive and direct-drive ICF studies[26–28], including both theoretical and experimental studies on Shenguang series laser facility. In RDMG, we solve the two-temperature hydrodynamic equations coupled with a multi-group radiation transfer equation. The multi-group radiation transfer equation is solved with S-N discrete coordinate scheme, and the energy coupling of radiation with matter is resolved by the matrix operator splitting method [29]. The laser energy deposition via inverse bremsstrahlung is calculated with a three-dimensional ray tracing package. The electron thermal conduction is treated by the Spitzer-Härm model [30, 31] with a flux limiter [32] which is usually taken as 0.08 in our simulations. The thermodynamic quantities are derived either from the ideal gas model or from data of realistic equation of state. In this work, we take 120 groups in solving the multi-group radiation transfer equation.

We consider a typical ignition laser pulse shape used in CH Rev5 design for the National Ignition Facility [33], which is presented in Fig. 1. The peak laser intensity is taken as 5×10^{14} W/cm². As shown, the pre-pulse finishes at around 16 ns

TABLE I: Parameters of laser and target in all models. Here, the laser pulse of 4ω - 2ω means that it takes 4ω laser for the pre-pulse and 2ω laser for the main-pulse. The foam-solid Au is composed by two parts: a foam part with $\rho_0 = 0.05$ g/cm³ and $\Delta = 40$ μ m, and a solid part with $\rho_0 = 19.24$ g/cm³ and $\Delta = 39$ μ m, with the foam part facing to the laser source. For the solid Au, $\rho_0 = 19.24$ g/cm³ and $\Delta = 40$ μ m.

Model	Laser pulse	Au plane target
I	3ω	Solid
II	4ω	Solid
III	2ω	Solid
IV	4ω - 2ω	foam-solid

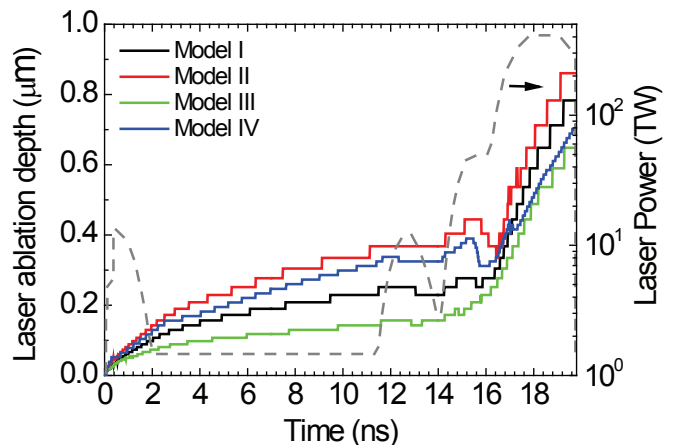


FIG. 1: (color online) Ignition pulse shape used in CH Rev5 design [33] (dashed grey line) and temporal evolutions of the laser ablation depth for all models (solid lines).

where it is 49 TW, and then the main-pulse begins. Therefore, our 4ω - 2ω pulse for this work is 4ω laser before 16 ns and 2ω laser thereafter. The four models we consider in simulations are given in the table. In model I, II and III, it is a solid Au plane target driven by 2ω , 3ω and 4ω lasers, respectively. In model IV, it is a foam-solid Au plane target driven by the 4ω - 2ω laser. The solid target has a thickness Δ of 40 μ m with $\rho_0 = 19.24$ g/cm³. The "foam-solid" target is composed by two parts: a foam part with $\rho_0 = 0.05$ g/cm³ and $\Delta = 40$ μ m and a solid part with $\rho_0 = 19.24$ g/cm³ and $\Delta = 39$ μ m, with the foam part facing to the laser source. The areal density of the foam part equals to a solid layer with 19.24 g/cm³ in density and 1 μ m in thickness. The reason for taking such a thickness for the foam part is because the laser ablation depth is approximately 1 μ m for Au driven by the CH Rev5 ignition laser pulse. We use such a thin foam layer only for the laser deposition region just to investigation whether the foam can help to increase the laser to x-ray conversion efficiency under the 4ω - 2ω pulse as compared to the solid Au under the 3ω pulse. Moreover, we take $\Delta = 39$ μ m for the solid part of the foam-solid Au while $\Delta = 40$ μ m for the solid Au, just to keep the same areal density for both targets, as mentioned in Sec. I.

III. SIMULATIONS AND DISCUSSIONS

In in-direct drive approach, the laser absorption efficiency, the laser to x-ray conversion efficiency, the x-ray output and its spectrum are very important for hohlraum energetics and capsule implosion performances, while they are strongly connected to both laser and target parameters. In this section, we present and compare the simulation results from RDMG for the four models .

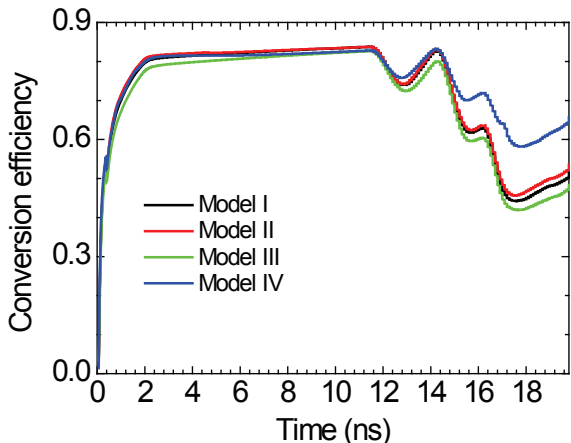


FIG. 2: (color online) Temporal evolutions of the laser to x-ray conversion efficiency for all models.

The laser ablation depth Δ_L is decided not only by laser intensity and laser wavelength, but also by the initial density of target [34]. Presented in Fig. 1 is Δ_L for all models. Here, we use 19.24 g/cm^3 as the nominated density of the foam part and calculate Δ_L under this nominated density for model IV. The results are discussed below. (1) For the same target, Δ_L strongly depends on λ_L , and it is smaller at a longer λ_L . For the first three models, Δ_L is about $0.7 \mu\text{m}$ at 2ω , $0.78 \mu\text{m}$ at 3ω and $0.86 \mu\text{m}$ at 4ω at the end of the laser pulse. (2) Δ_L is more sensitive to λ_L during pre-pulse than main-pulse. Fitting from the first three models, we have $\Delta_L \propto \lambda_L^{-3/2}$ for pre-pulse and $\Delta_L \propto \lambda_L^{-1/2}$ for the main-pulse. (3) During the main-pulse, Δ_L is mainly decided by λ_L while relatively insensitive to ρ_0 . Models III and IV have almost the same Δ_L because they both use 2ω during the main-pulse.

For the laser absorption efficiency η_{aL} given in this paper, we only consider the laser absorption via inverse bremsstrahlung. The laser backscatter caused by LPI is not taken into considerations in this work, because present simulation results, including results from 2D codes, cannot adequately describe the observed LPI [35] and therefore a qualitatively study on backscatter requires the experimental measurements. From our simulations, η_{aL} is higher at a shorter λ_L , and it is higher inside the foam-solid Au than inside the solid Au under the same laser pulse with same λ_L . Nevertheless, η_{aL} rises sharply as time, reaching 99% in less than 1 ns and approaching 100% in all models. Therefore, η_{aL} has few difference among the four models.

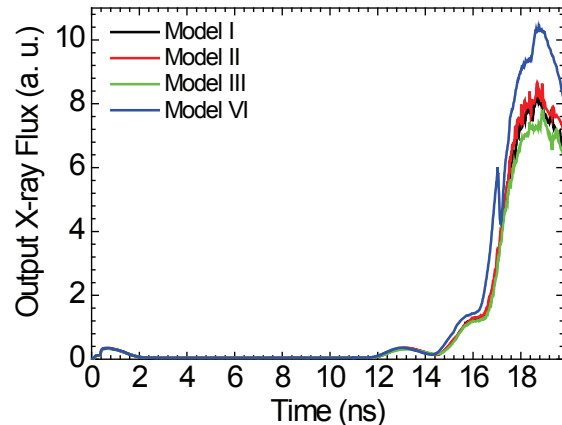


FIG. 3: (color online) Temporal evolutions of the output x-ray flux emitted from the target surface where the laser is deposited.

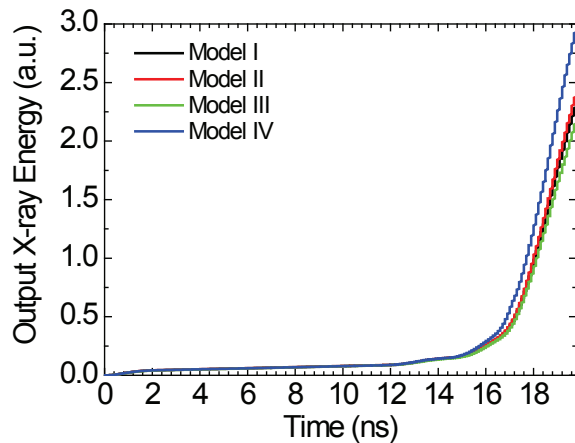


FIG. 4: (color online) Output x-ray energy emitted from the target surface where the laser is deposited.

Presented in Fig. 2 is the temporal evolutions of η_{LX} for all models. The results are discussed below. (1) η_{LX} rises rapidly during the first step of the ignition laser pulse and reaches around 80% at about 2ns for all models. (2) η_{LX} drops at the frontiers of all later steps when the laser power rises steeply. (3) η_{LX} is lower at a longer λ_L , but it can be remarkably increased by the foam layer of the foam-solid Au. From the results of the first three models which use solid Au, η_{LX} is 52.3% at 4ω , 50% at 3ω and 47% at 2ω at the end of the laser pulse. However, the foam layer of the foam-solid Au can remarkably increase η_{LX} at 2ω , and can make η_{LX} even obviously higher than 4ω with solid Au. In model IV, η_{LX} is about 64% at the end of laser pulse, which is 36% higher than the 2ω model, 28% higher than the 3ω model, and 22% higher than the 4ω model with solid Au. As a result of the increased η_{LX} in the foam-solid Au, both output x-ray flux and x-ray energy driven by 2ω laser are be remarkably increased in model IV, and they can be even higher than the cases driven

by 3ω and 4ω with solid Au. From Fig. 3 and Fig. 4, the output x-ray flux and x-ray energy of model IV is about 36% higher than the 2ω model, 28% higher than the 3ω model, and 22% higher than the 4ω model which all use solid Au.

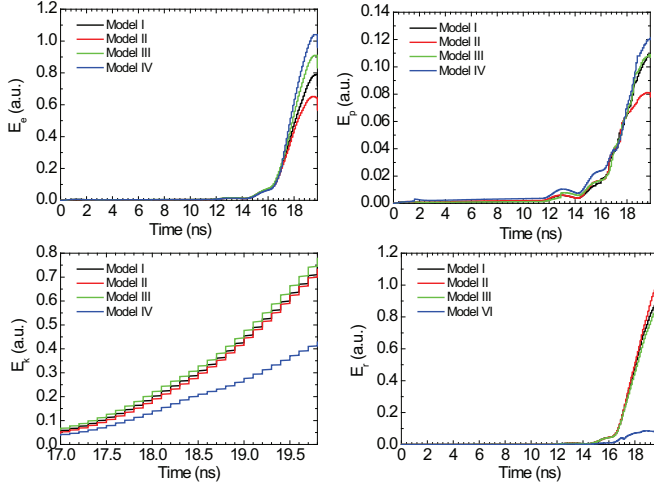


FIG. 5: (color online) Temporal evolutions of electronic thermal energy E_e , the ionic potential energy E_p , the plasma kinetic energy E_k , and the radiation energy E_r for all models.

In order to understand why the x-ray output can be increased with a foam layer, we compare all kinds of energies of the laser ablation region among the four models, where the electronic density is lower than the critical density and the laser can be deposited. Recall that in model IV, the foam layer faces to the laser source and has a thickness equal to the laser ablation depth. Hence, the main influences caused by the foam layer mainly happen in the laser ablation region. Presented in Fig.5 is temporal evolutions of the electronic thermal energy E_e , the ionic potential energy E_p , the plasma kinetic energy E_k , and the radiation energy E_r for all models. Here, we take an arbitrary unit for these energies. As shown, all E_e , E_p , E_k and E_r depend on both λ_L and ρ_0 , but with very different behaviors. Notice that we have neglected the ionic thermal energy in Fig.5 because it is very small in the laser ablation region and can be neglected as compared to all other kinds of energies.

According to our simulation results, both E_e and E_p are higher at a longer λ_L , and they are higher in the foam-solid Au than in the solid Au. From Fig.5, E_e is 0.92, 0.79 and 0.65 in the solid Au driven by the laser pulses at 2ω , 3ω and 4ω , respectively; and it is 1.04 in the foam-solid Au under the 4ω - 2ω pulse. Again from Fig.5, E_p is about 0.11, 0.11 and 0.08 in the solid Au driven by the laser pulses at 2ω , 3ω and 4ω , respectively; and it is 0.12 in the foam-solid Au under the 4ω - 2ω pulse. However, the differences of E_e and E_p among these four models are not remarkable. Nevertheless, these results are connected to the electron thermal conduction model used in our simulations, and it is worth to be checked by future simulations with more accurate physics models.

In contrast, both E_k and E_r are remarkably decreased by

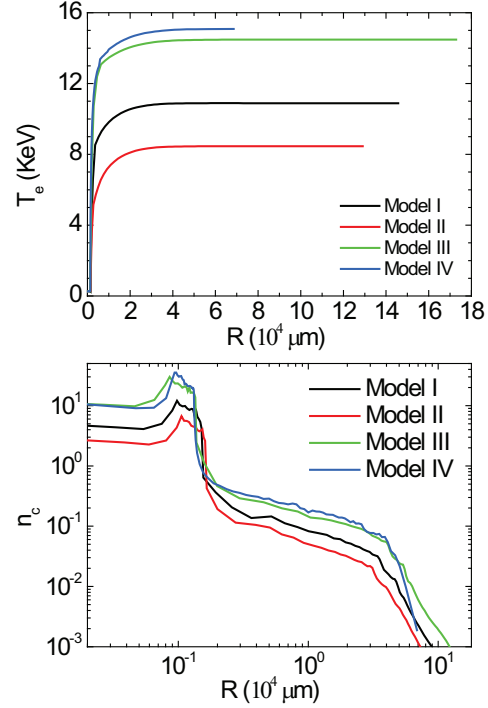


FIG. 6: (color online) Spatial distributions of electronic temperature T_e and electronic density n_e , which is normalized to the critical density of corresponding λ_L , at 19.5 ns before the laser pulse ends.

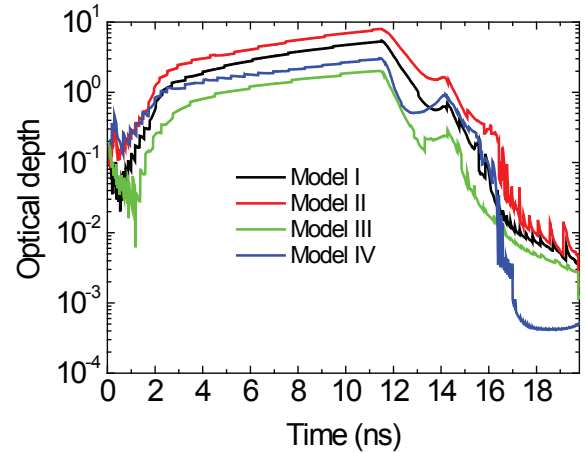


FIG. 7: (color online) Temporal evolutions of the optical depth for all models.

using the foam-solid Au as compared to the solid Au. Here, we only compare model IV with model I which uses solid Au driven by 3ω laser, because the differences among the first three models are small. From Fig.5, E_k of model IV is 43% lower than model I, and E_r of model IV is about 92% lower than model I. It means that in the laser ablation region, the kinetic energy of model IV is down by about half from model I, and the radiation energy of model IV decreases by an order of magnitude over model I. In the following, we discuss the

reasons for such remarkable decreases of E_k and E_r , respectively.

There are two reasons for the decrease of E_k in the foam-solid Au. One reason is due to a thinner Δ_L in the foam than in the solid, as shown in Fig.1. Another one is due to the propagation competition between the radiation front and sonic speed. According to Refs.[18] and [19], the radiation front propagates subsonically and part of the absorbed energy is wasted by the flow kinetic energy for the solid target, while the front velocity is supersonic and can devote almost all of the absorbed energy to heating the material for the foam target. Presented in Fig.6 is the spatial distributions of electron temperature T_e and normalized electron density n_e at 19.5 ns before the laser pulse ends. As presented, model IV with foam-solid Au has a much shorter expansion than the solid target models. In addition, T_e is higher at a longer λ_L ; and T_e in model IV is close to model III, because they both use 2ω laser during the main-pulse. Moreover, the spacial distributions of n_e are sensitive to λ_L , and n_e is obviously lower at a shorter λ_L . This is the reason why LPI levels are lower at 3ω and 4ω . As it is shown, n_e of model IV is close to that of model III at $n_e \geq 0.02$, again because they both use 2ω laser during the main-pulse. Notice that a lower LPI backscatters of model IV can be expected than model III, because they have a similar spacial distribution of n_e while model IV has a higher T_e than model III. Nevertheless, as we have mentioned above, the LPI levels needs to be measured by experiments for the quantitatively study.

The reason for the decrease of E_r inside the foam-solid Au has not been discussed in previous publications, but it is not surprising. Presented in Fig.7 is the temporal evolutions of the optical depth for all models. As shown, optical depth of the foam-solid is remarkably decreased about 4 to 7 times as compared to the solid models, and this is due to its shorter expansion and higher T_e than the solid models.

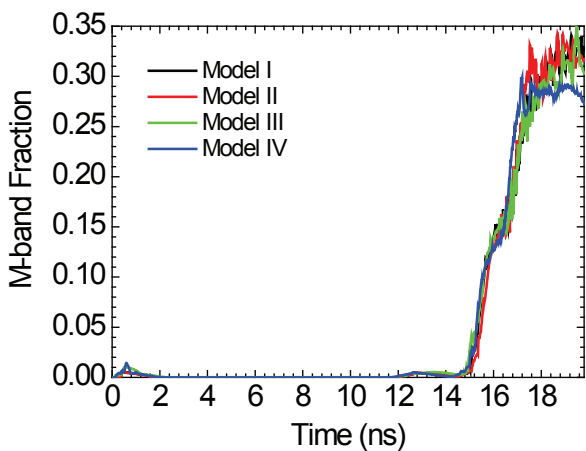


FIG. 8: (color online) M-band fractions of the output x-ray flux for all models.

Finally, it is worth to compare the M-band fraction f_M between the foam-solid target and the solid target, because the x-ray spectrum is very important for the implosion

performances[36]. The portion of the X-ray flux above 1.8 keV generated in the laser-heated Au can preheat capsule and arouse hydrodynamic instabilities [1, 27]. In our simulations, we define the emissions between 1.8 keV and 4 keV as the M-band of Au. Presented in Fig. 8 is temporal evolutions of f_M for all models. As shown, f_M is very small before 14 ns, but later it increases rapidly with laser power and reaches about 15% at around 16 ns for all models. For the first three models with the solid Au, f_M varies as λ_L while the differences are small. However, f_M is more sensitive to ρ_0 . For model IV which uses the foam-solid target, f_M obviously decreases as compared to the results of the solid Au. At around 19 ns, f_M is around 34% in the first three models, while it is around 29% in models IV. Therefore, f_M can be clearly decreased with the foam-solid target.

In this work, we also simulate a model in which the foam-solid Au is driven by a 2ω laser during whole ignition pulse and compare its simulation results with model IV. The comparisons show that their results are close, which is reasonable because they all use 2ω for the main-pulse. In addition, we also consider the foam-solid targets with $\rho_0 = 0.25 \text{ g/cm}^3$ and $\Delta = 80 \mu\text{m}$ or $\rho_0 = 1 \text{ g/cm}^3$ and $\Delta = 20 \mu\text{m}$ for the foam part, and their simulation results have no big differences from what we have for model IV. In fact, to search the optimum ρ_0 of foam for ignition hohlraum design, one should study and compare the x-ray radiations inside the hohlraums with various foam density under an ignition laser drive by using 2D or 3D simulations and performing systematic experiments with both modest energy (SGIII and Omega) and MJ scale lasers such as the NIF and LMJ. In future studies, a thick foam should be used, which thickness can cover both laser ablated region and radiation ablated region.

IV. SUMMARY

We have proposed to drive a foam hohlraum wall with an ignition laser pulse by the 4ω - 2ω ignition pulse, in order to take the advantage of 4ω laser in its low LPI during the pre-pulse, the advantage of 2ω laser in its relatively high energy output and low damage threshold during the main-pulse, and the advantage of foam in its high η_{LX} , high η_{HC} and relatively low M-band fraction in its radiation spectrum. The advantage of foam in a higher η_{HC} was predicted and demonstrated in previous publications. In this work, we have demonstrated the advantage of foam in a higher η_{LX} by comparing the laser ablations between a solid target and a foam-solid target under an ignition laser pulse with our 1D simulations. As a result, η_{LX} can be increased by 28% in the foam-solid Au under the 4ω - 2ω pulse as compared to a pure solid Au under a 3ω laser. Our studies have shown that the increase of η_{LX} of the foam-solid Au is due to the decreases of its kinetic energy and radiation energy as compared to a solid Au, and the decrease of the radiation energy is caused by the shorter optical depth inside a foam. In addition, a lower LPI levels is expected from foam than from solid because of its higher electronic temperature in the laser deposited region.

Because 2ω laser energy delivered to drive a fusion target

can exceed 3ω by a factor of about 1.1 to 1.2, together with the increased η_{LX} , η_{HC} and the decreased LPI levels inside the foams, it may provide a larger and flexible design space for ignition with a foam hohlraum wall and a 4ω - 2ω laser pulse. Because of the low damage threshold of the 2ω laser at high power laser, we can therefore expect a remarkable increase of shot number at high laser energy power on a laser ignition facility for ignition study. Nevertheless, it is mandatory to have experiments for an understanding and demonstration of acceptable LPI levels and target coupling physics of 2ω lasers.

Acknowledgments

The authors wish to acknowledge the beneficial help from Guoli Ren, Yaohua Chen, Yongsheng Li, and Wanguo Zheng. This work is supported by the Development Foundation of CAEP (Grant No. 2013A0102002) and the National Natural Science Foundation of China (Grant No. 11475033).

-
- [1] J. D. Lindl, B. A. Hammel, and B. G. Logan, D. D. Meyerhofer, S. A. Payne and J. D. Sethian, *Plasma Phys. Control. Fusion* **45**, A217-A234 (2003).
- [2] J. D. Lindl, O. Landen, J. Edwards, E. Moses, and NIC Team, "Review of the National Ignition Campaign 2009-2012", *Phys. Plasmas* **21**, 020501 (2014).
- [3] W. Zheng, X. Wei, Q. Zhu, F. Jing, D. Hu, J. Su, K. Zheng, X. Yuan, H. Zhou, W. Dai, W. Zhou, F. Wang, D. Xu, X. Xie, B. Feng, Z. Peng, L. Guo, Y. Chen, X. Zhang, L. Liu, D. Lin, Z. Dang, Y. Xiang, and X. Deng, *High Power Laser Science and Engineering* **4**, doi:10.1017/hpl.2016.20 (2016).
- [4] K. Lan, J. Liu, Z. Li, X. Xie, W. Huo, Y. Chen, G. Ren, C. Zheng, D. Yang, S. Li, Z. Yang, L. Guo, S. Li, M. Zhang, X. Han, C. Zhai, L. Hou, Y. Li, K. Deng, Z. Yuan, X. Zhan, F. Wang, G. Yuan, H. Zhang, B. Jiang, L. Huang, W. Zhang, K. Du, R. Zhao, P. Li, W. Wang, J. Su, X. Deng, D. Hu, W. Z. H. Jia, Y. Ding, W. Zheng, X. He, *Matter and Radiation at Extremes* **1**, 8 (2016).
- [5] E. M. Campbell, R. Cauble, and B. A. Remington, *AIP Conference Proceedings* **429**, 3 (1998).
- [6] J. Giorla, J. Bastian, C. Bayer, B. Canaud, M. Casanova, F. Chaland, C. Cherfils, C. Clique, E. Dattolo, P. Fremerye, D. Galmiche, F. Garaude, P. Gauthier, S. Laffite, N. Lecler, S. Liberatore, P. Loiseau, G. Malinie, L. Masse, A. Masson, M. C. Monteil, F. Poggi, R. Quach, F. Renaud, Y. Saillard, P. Seytor, M. Vandenboomgaerde, J. Van der Vliet, and F. Wagon, *Plasma Phys. Control. Fusion* **48** B75 (2006).
- [7] P. Neumayer, R. L. Berger, D. Callahan, L. Divol, D. H. Froula, R. A. London, B. J. MacGowan, N. B. Meezan, P. A. Michel, J. S. Ross, C. Sorce, K. Widmann, L. J. Suter, and S. H. Glenzer, *Phys. Plasmas* **15**, 056307 (2008).
- [8] J. L. Kline, S. H. Glenzer, R. E. Olson, L. J. Suter, K. Widmann, D. A. Callahan, S. N. Dixit, C. A. Thomas, D. E. Hinkel, E. A. Williams, A. S. Moore, J. Celeste, E. Dewald, W. W. Hsing, A. Warrick, J. Atherton, S. Azevedo, R. Beeler, R. Berger, A. Conder, L. Divol, C. A. Haynam, D. H. Kalantar, R. Kauffman, G. A. Kyrala, J. Kilkenny, J. Liebman, S. Le Pape, D. Larson, N. B. Meezan, P. Michel, J. Moody, M. D. Rosen, M. B. Schneider, B. Van Wronterghem, R. J. Wallace, B. K. Young, O. L. Landen, and B. J. MacGowan, *Phys. Rev. Lett.* **106**, 085003 (2011).
- [9] D. H. Froula, L. Divol, N. B. Meezan, S. Dixit, J. D. Moody, P. Neumayer, B. B. Pollock, J. S. Ross, and S. H. Glenzer, *Phys. Rev. Lett.* **98**, 085001 (2007).
- [10] C. A. Haynam, P. J. Wegner, J. M. Auerbach, M. W. Bowers, S. N. Dixit, G. V. Erbert, G. M. Heestand, M. A. Henesian, M. R. Hermann, K. S. Jancaitis, K. R. Manes, C. D. Marshall, N. C. Mehta, J. Menapace, E. Moses, J. R. Murray, M. C. Nostrand, C. D. Orth, R. Patterson, R. A. Sacks, M. J. Shaw, M. Spaeth, S. B. Sutton, W. H. Williams, C. C. Widmayer, R. K. White, S. T. Yang, and B. M. Van Wronterghem, *Appl. Opt.* **46**, 3276 (2007).
- [11] L. J. Suter, S. Glenzer, S. Haan, B. Hammel, K. Manes, N. Meezan, J. Moody, M. Spaeth, and L. Divol K. Oades and M. Stevenson, *Phys. Plasmas* **11**, 2738 (2004).
- [12] C. Niemann, R. L. Berger, L. Divol, D. H. Froula, O. Jones, R. K. Kirkwood, N. Meezan, J. D. Moody, J. Ross, C. Sorce, L. J. Suter, and S. H. Glenzer, *Phys. Rev. Lett.* **100**, 045002 (2008).
- [13] S. Depierreux, D. T. Michel, V. Tassin, P. Loiseau, C. Stenz, and C. Labaune, *Phys. Rev. Lett.* **103**, 115001 (2009).
- [14] R. M. Stevenson, K. Oades, B. R. Thomas, M. Schneider, G. E. Slark, L. J. Suter, R. Kauffman, D. Hinkel, and M. C. Miller, *Phys. Rev. Lett.* **94**, 055006 (2005).
- [15] C. Labaune, *Nature Phys.* **3**, 680 (2007).
- [16] S. Depierreux, P. Loiseau, D. T. Michel, V. Tassin, C. Stenz, P.-E. Masson-Laborde, C. Goyon, V. Yahia, and C. Labaune, *Phys. Plasmas* **19**, 012705 (2012).
- [17] Z. Li, J. Zheng, X. Jiang, Z. Wang, D. Yang, H. Zhang, S. Li, Q. Yin, F. Zhu, P. Shao, X. Peng, F. Wang, L. Guo, P. Yuan, Z. Yuan, L. Chen, S. Liu, S. Jiang, and Y. Ding, *Phys. Plasmas* **19**, 062703 (2012).
- [18] M. D. Rosen and J. H. Hammer, *Phys. Rev. E.* **72**, 056403 (2005).
- [19] P. E. Young, M. D. Rosen, J. H. Hammer, W. S. Hsing, S. G. Glendinning, R. E. Turner, R. Kirkwood, J. Schein, C. Sorce, J. H. Satcher, Jr., A. Hamza, R. A. Reibold, R. Hibbard, O. Landen, A. Reighard, S. McAlpin, M. Stevenson, and B. Thomas, *Phys. Rev. Lett.* **101**, 035001 (2008).
- [20] Y. Dong, W. Shang, J. Yang, L. Zhang, W. Zhang, Z. Li, L. Guo, X. Zhan, H. Du, B. Deng, and Y. Pu, *Phys. Plasmas* **20**, 123305 (2013).
- [21] L. Zhang, Y. Ding, S. Jiang, J. Yang, H. Li, L. Kuang, Z. Lin, L. Jing, L. Li, B. Deng, Z. Yuan, T. Chen, G. Yuan, X. Tan, and P. Li, *Phys. Plasmas* **22**, 110703 (2015).
- [22] L. Zhang, Y. Ding, Z. Lin, H. Li, L. Jing, Z. Yuan, Z. Yang, X. Tan, L. Kuang, W. Zhang, L. Li, P. Li, G. Yuan, S. Jiang and B. Zhang, *Nucl. Fusion* **56**, 036006 (2016).
- [23] L. Zhang, Y. Ding, J. Yang, S. Wu, and S. Jiang, *Phys. Plasmas* **18**, 033301 (2011).
- [24] Y. Dong, L. Zhang, J. Yang, and W. Shang, *Phys. Plasmas* **20**, 123102 (2013).
- [25] T. Feng, D. Lai, and Y. Xu, *Chinese J. Comput. Phys.* **16**, 199-205 (1999).
- [26] Y. Xu, S. Jiang, D. Lai, W. Pei, Y. Ding, T. Chang, K. Lan, S. Li, and T. Feng, *Laser and Particle Beams* **24**, 495(2006)
- [27] Y. Li, W. Y. Huo and K. Lan, *Phys. Plasmas* **18**, 022701 (2011); W. Y. Huo, K. Lan, Y. Li, D. Yang, S. Li, X. Li, C. Wu, G. Ren, Y. Zhao, S. Zou, W. Zheng, P. Gu, M. Wang, R. Yi, X. Jiang, T. Song, Z. Li, L. Guo, Y. Liu, X. Zhan, F. Wang, X. Peng, H. Zhang, J. Yang, S. Liu, S. Jiang, and Y. Ding, *Phys. Rev. Lett.*

- 109**, 145004(2012).
- [28] Y. Xu, S. Wu, and W. Zheng, *Phys. Plasmas* **22**, 042708 (2015).
- [29] T. Feng, D. Lai, Y. Xu, and J. Li, *Annual Reports of China Academy of Engineering Physics 1998* (Atomic Energy Press, Chengdu, 1998), p. 286 (in Chinese).
- [30] R. S. Cohen, L. Spitzer, and P. M. Routly, *Phys. Rev.* **80**, 230 (1950).
- [31] L. Spitzer and R. Härm, *Phys. Rev.* **89**, 977 (1953).
- [32] R. C. Malone, R. L. McCrory, and R. L. Morse, *Phys. Rev. Lett.* **12**, 721 (1975).
- [33] S. W. Haan, J. D. Lindl, D. A. Callahan, D. S. Clark, J. D. Salmonson, B. A. Hammel, L. J. Atherton, R. C. Cook, M. J. Edwards, S. Glenzer, A. V. Hamza, S. P. Hatchett, M. C. Herrmann, D. E. Hinkel, D. D. Ho, H. Huang, O. S. Jones, J. Kline, G. Kyrala, O. L. Landen, B. J. MacGowan, M. M. Marinak, D. D. Meyerhofer, J. L. Milovich, K. A. Moreno, E. I. Moses, D. H. Munro, A. Nikroo, R. E. Olson, K. Peterson, S. M. Pollaine, J. E. Ralph, H. F. Robey, B. K. Spears, P. T. Springer, L. J. Suter, C. A. Thomas, R. P. Town, R. Vesey, S. V. Weber, H. L. Wilkens, and D. C. Wilson, *Phys. Plasmas* **18**, 051001 (2011).
- [34] S. Atzeni, J. Meyer-ter-Vehn, *The Physics of Inertial Fusion* (Oxford Science, Oxford, 2004).
- [35] J. L. Kline, D. A. Callahan, S. H. Glenzer, N. B. Meezan, J. D. Moody, D. E. Hinkel, O. S. Jones, A. J. MacKinnon, R. Bennedetti, R. L. Berger, D. Bradley, E. L. Dewald, I. Bass, C. Bennett, M. Bowers, G. Brunton, J. Bude, S. Burkhart, A. Condor, J. M. Di Nicola, P. Di Nicola, S. N. Dixit, T. Doeppner, E. G. Dzenitis, G. Erber, J. Folta, G. Grim, S. Lenn, A. Hamza, S. W. Hann, J. Heebner, M. Henesian, M. Hermann, D. G. Hicks, W. W. Hsing, N. Izumi, K. Jancaitis, O. S. Jones, D. Kalantar, S. F. Khan, R. Kirkwood, G. A. Kyrala, K. LaFortune, O. L. Landen, L. Lain, D. Larson, S. Le Pape, T. Ma, A. G. MacPhee, P. A. Michel, P. Miller, M. Montincelli, A. S. Moore, A. Nikroo, M. Nostrand, R. E. Olson, A. Pak, H. S. Park, M. B. Schneider, M. Shaw, V. A. Smalyuk, D. J. Strozzi, T. Suratwala, L. J. Suter, R. Tommasini, R. P. J. Town, B. Van Wousterghem, P. Wegner, K. Widmann, C. Widmayer, H. *Phys. Plasmas* **20**, 056314 (2013).
- [36] R. E. Olson, R. J. Leeper, A. Nobile, and J. A. Oerte, *Phys. Rev.Lett.* **91**, 235002 (2003).